Bioactive Materials 3 (2018) 87–96

Contents lists available at ScienceDirect

Bioactive Materials

journal homepage: http://www.keaipublishing.com/en/journals/bioactive-materials/

Construction of versatile multilayered composite nanoparticles from a customized nanogel template

Jian Zhang [a, b, 1], Jinpeng Jia [c, 1], Jimin P. Kim [d], Fei Yang [a, b], Xing Wang [a], Hong Shen [a], Sijia Xu [a, b], Jian Yang [d], Decheng Wu [a, b, *]

[a] Beijing National Laboratory for Molecular Sciences, State Key Laboratory of Polymer Physics & Chemistry, Institute of Chemistry, Chinese Academy of Sciences, Beijing, China
[b] University of Chinese Academy of Sciences, Beijing, China
[c] Department of Orthopaedics, General Hospital of Chinese People's Liberation Army, Beijing, China
[d] Department of Biomedical Engineering, Materials Research Institute, The Huck Institutes of the Life Sciences, The Pennsylvania State University, University Park, PA, USA

ARTICLE INFO

Article history:
Received 9 May 2017
Received in revised form
9 June 2017
Accepted 26 June 2017
Available online 1 July 2017

Keywords:
Multilayer
Multifunctional
Nanoparticles
Controlled
Nanogel template

ABSTRACT

We present a highly adaptable design platform for multi-responsive, multilayered composite nanoparticles (MC-NPs) with fine-tunable functional layers. A flexible disulfide-linked nanogel template is obtained by a controlled *in-situ* gelation method, enabling a high degree of control over each successive layer. From this template, we optimize "smart" biomaterials with biofunctional surfaces, tunable drug release kinetics, and magnetic or pH-responsive functionality, fabricated into MC-NPs for targeted drug release and periosteum-mimetic structures for controlled rhBMP-2 release towards bone tissue formation *in-vivo*. Such a versatile platform for the design of MC-NPs is a powerful tool that shows considerable therapeutic potential in clinical fields such as oncology and orthopedics.

1. Introduction

Multilayered composite nanoparticles (MC-NPs) are gaining a significant interest in the pharmaceutical industry with applications ranging from controlled drug delivery to theranostic imaging [1–8]. The fabrication process typically involves layer-by-layer deposition of biologically functional surfaces onto silica, gold, or polystyrene templates, thereby leading to versatile and tunable compositions of NPs. These multilayered structures allow unprecedented control over shell-mediated biological interactions, demonstrated in the landmark work of Richtering et al. in the fabrication of stimuli-responsive microgels with unique core/shell behavior [9,10]. However, reported fabrication methods of MC-NPs to date, including condensation from vapor, chemical coating, and solid-state processes, offer little control over the properties of individual layers so that morphology, elasticity, and particle size cannot be independently adjusted for each layer [11–14]. The key challenge in the design flexibility and complexity of MC-NPs is the difficulty of creating a versatile template with easily adjustable properties.

Recently, we reported a controlled *in-situ* gelation method for fabrication of hydrogels and hydrogel particles [15,16]. Adjustment of the gelation time followed by seed emulsion allowed a high degree of control over each layer, yielding a biocompatible multilayered nanogels with tunable size, swelling capacity, and degree of crosslinking. Inspired from the facile fabrication of customized multilayered nanogels, we hypothesized that this general approach could be applied towards the production of multi-responsive MC-NPs. In this work, we first establish a versatile design platform for MC-NPs, where fabrication criteria included various stimuli-responsive layers, biofunctional surfaces, and adjustment of gelation times. With these fundamental understandings, we next specifically design "smart" MC-NPs responsive to magnetic and pH stimuli, and explore further applications as controlled-release rhBMP-2 carriers in periosteum-mimetic structures for bone

* Corresponding author. Beijing National Laboratory for Molecular Sciences, State Key Laboratory of Polymer Physics & Chemistry, Institute of Chemistry, Chinese Academy of Sciences, Beijing, 100190, China.
E-mail address: dcwu@iccas.ac.cn (D. Wu).
Peer review under responsibility of KeAi Communications Co., Ltd.
[1] These two authors contributed equally to this article.

http://dx.doi.org/10.1016/j.bioactmat.2017.06.003

tissue formation *in-vivo* (Fig. 1).

2. Materials and methods

2.1. Materials

1-(2-aminoethyl)piperazine (AEPZ, Aldrich), N,N'-bis(acryloyl) cystamine (BAC, Fluka), poly(ethylene glycol) methyl ether (Mn: 750, Aldrich), span80 (J&K) and tween80 (J&K) were purchased and used without further purification. α-Amino-ω-methoxy-poly(-ethylene glycol) was prepared from poly(ethylene glycol) methyl ether according to literature [17]. L-lactide and glycolide were purchased from PURAC (the Netherlands) and purified by recrystallization in ethyl acetate (Beijing Tonghua fine chemicals company) twice. Poly(lactic-*co*-glycolic acid) (PLGA) was prepared by ring-opening polymerization of L-lactide and glycolide under 65 Pa in sealed glass ampoules at 180 °C for 20 h in the presence of stannous octoate as catalyst (0.05 wt%). The raw PLGA (50/50) (85,000) (Molecular weights were determined by GPCmax VE-2001 gel-permeation chromatography) was purified by dissolving in chloroform and re-precipitation from ethanol, followed by drying in vacuum at room temperature for 48 h. The 1,4-dioxane and other reagents were obtained from Beijing Chemical Reagents Company, China and directly used without further treatment. The 1,4-dioxane used in here was not chromatographically pure. All other chemicals were purchased from Sigma-Aldrich.

2.2. Synthesis of hyperbranched poly(BAC2-AEPZ1)-PEG (BAP)

The hyperbranched poly(BAC2-AEPZ1)-PEG (BAP) was synthesized by a one-pot, two-step Michael addition polymerization [15]. In detail, BAC (3.0 mmol) was dissolved in 10 mL of methanol at room temperature. AEPZ (1.5 mmol) was added dropwise to the solution while stirring, followed by rinsing with 2 mL of methanol. The mixture was stirred at 50 °C for about 6 days. 2.3 mmol of α-amino-ω-methoxy-PEG (Mn = 750) was added stirred at 60 °C for one week to seal terminal vinyl groups. The product was precipitated from the reaction using 200 mL of diethyl ether under vigorous stirring. The polymer was collected and purified by re-precipitation from a methanol solution into 100 mL of acetone containing 5 mL of 37% concentration HCl followed by drying under vacuum at 50 °C for 24 h. A water soluble hyperbranched poly(-amido amine), poly(BAC2-AEPZ1)-PEG (BAP), was obtained as depicted in Fig. 2.

2.3. Preparation of loose and compact nanogels

The inverse mini-emulsion method was adopted for producing loose and compact nanogels (Fig. 3). In detail, decane was selected as the organic continuous phase, and a mixture of span80/tween80 (0.49 g/0.51 g) with a weight ratio of 49: 51 was used as surfactant. The organic mixture containing decane and surfactants was formulated with the decane/surfactant weight ratio of 19 g: 1 g. The aqueous solution was prepared by dissolving 10 mg of BAP in 25 μL of deionized water, and basified using 7.8 μL of 5 M Sodium hydroxide (NaOH). Then 32.8 μL of the aqueous solution was immediately added into 25 mL of the organic mixture, stirring at 700 rpm to yield a stable mini-emulsion. The emulsion was injected with 2 mL of deionized water to lower the pH and terminate gelation after a predetermined time ranging from 4 to 10 h. The emulsion was centrifuged at 1000 rpm for 1 min, and the upper surfactant and decane layers were discarded. The remaining liquid was dialyzed by deionized water to obtain pure, surfactant-free nanogels.

2.4. Preparation of nanogel/silica NPs

The template method was utilized for producing loose and compact double-layered nanoparticles. To prepare the template, decane was selected as the organic continuous phase, and a mixture of span80/tween80 (0.49 g/0.51 g) was used as surfactant. The organic mixture containing decane and surfactants was formulated with the decane/surfactant weight ratio of 19:1. The aqueous solution was prepared by dissolving 10 mg of BAP in 25 μL of deionized water, and basified using 7.8 μL of 5 M NaOH. Then 32.8 μL of the aqueous solution was immediately added into 25 mL of the organic mixture, stirring at 700 rpm to yield a stable mini-emulsion. The emulsion was injected with 2 mL of deionized water to lower the pH and terminate gelation after a predetermined

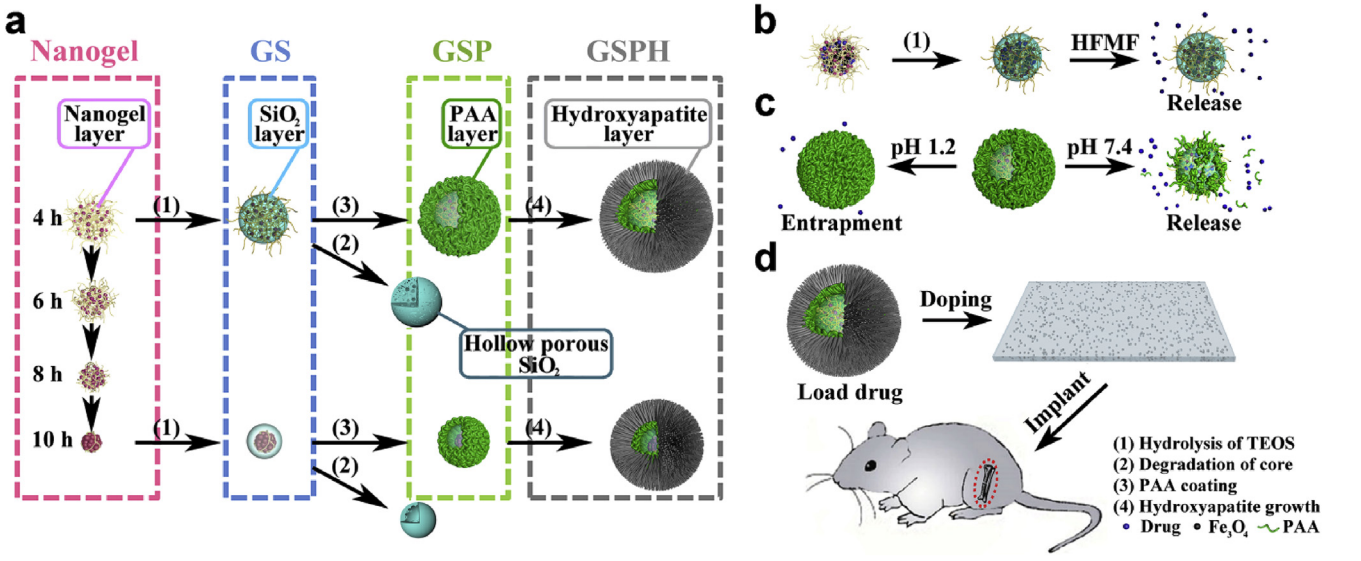

Fig. 1. The fabrication process of various multilayered composite nanoparticles. a) Controlled formation of the nanogel core, silica shell-nanogel core NPs (GS), pH-responsive poly-(acrylic acid) (PAA)-silica-nanogel NPs (GSP), and hydroxyapatite (HA) coated PAA-silica-nanogel NPs (GSPH). b) Magnetic-responsive release produced by magnetic silica-nanogel NPs under high-frequency alternating magnetic fields (HFMF). c) pH-responsive release of PAA-silica-nanogel NPs. d) *In-vivo* translation of multilayered composite nanoparticles toward periosteum-mimetic biomaterials for bone repair.

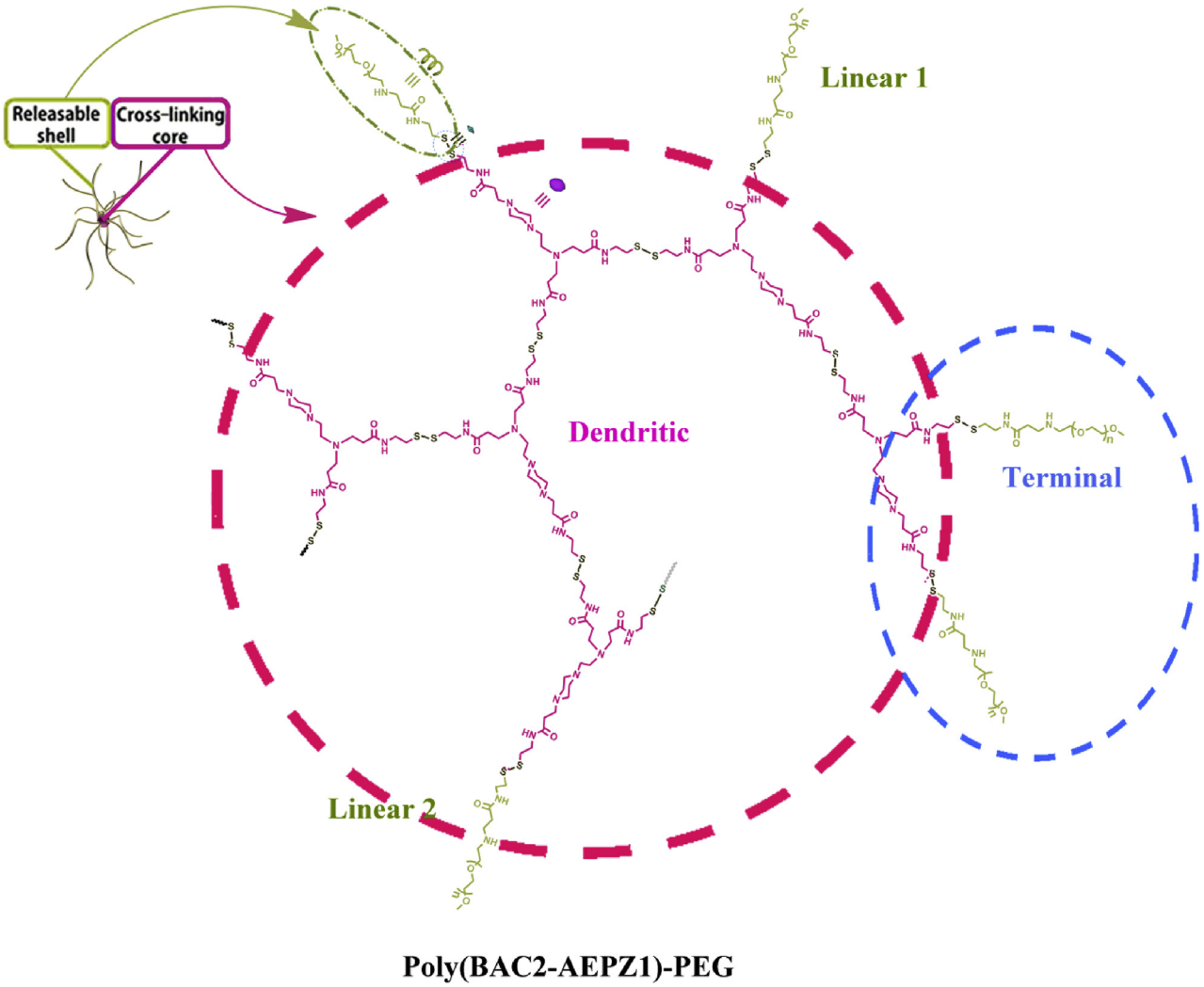

Fig. 2. Chemical structure of the polymer, poly(BAC2-AEPZ1)-PEG (BAP).

time ranging from 4 to 10 h. The emulsion was centrifuged at 1000 rpm for 1 min, and the upper surfactant and decane layers were discarded. The remaining liquid was dialyzed by deionized water for 30 min and mixed with 2 mL 27% ammonium hydroxide, and then injected into 4 mL ethanol containing 10 μL tetraethyl orthosilicate (TEOS), stirring at 300 rpm for 1 h to obtain the nanoparticles. After dialysis using deionized water, the nanoparticles were characterized by TEM and dynamic light scattering (DLS) spectrum (Zetasizer Nano ZS, Malvern).

To prepare silica capsules, nanogel/SiO_2 NPs with 4, 6, 8 and 10 h gelation cores were prepared as above, and then dialyzed by 1 × PBS containing 30 mM Glutathione (GSH) for 24 h, followed by further dialysis of the emulsion by deionized water for 3 days to obtain silica capsules, characterized thereafter by TEM and DLS.

2.5. Preparation of the magnetic-sensitive nanoparticles

In detail, 353.2 mg (1 mmol) ferric acetylacetonate was stirred with 30 mL of triethylene glycol and passed through N_2 for 10 min. Then the mixture was refluxed at 278 °C for 30 min. After the color of the mixture turned from red to brown, we precipitated the mixture in ethyl acetate 5 times to get pure Fe_3O_4 nanoparticles. The products were analyzed using transmission electron microscopy (TEM, JEOL JEM-2200FS) and powder X-ray diffraction spectroscopy (XRD, D/max 2500 VB2þ/PC, Rigaku).

To the organic mixture containing decane and surfactants describe above, an aqueous solution was added containing 10 mg of BAP and 7 mg of Fe_3O_4 nanoparticles in 25 μL of deionized water and 7.8 μL of 5M NaOH. Protocols for obtaining a mini-emulsion, gelation, and dialysis were followed as described above. To obtain magnetic nanogel NPs without a silica layer, we omitted the extra step of deionizing with ammonium hydroxide and injecting TEOS.

Characterization of magnetic nanogel/SiO_2 NPs (GFS) was performed by TEM analysis along with the superconducting quantum interference device (SQUID, MPMS-XL7, 298 K and ±6000 G). The Fe_3O_4 content was studied with derivative thermo-gravimetric analyzer (TGA; Pyris 1, Perkin Elmer) in air by observing the thermal weight loss of nanogels in the nanogel/SiO_2 NP and its magnetic counterpart.

2.6. Preparation of nanogel/SiO_2/poly(acrylic acid) NPs

Nanogel/SiO_2 NPs with 4, 6, 8, and 10 h gelation cores were prepared as above. Following dialysis to obtain pure silica-nanogel

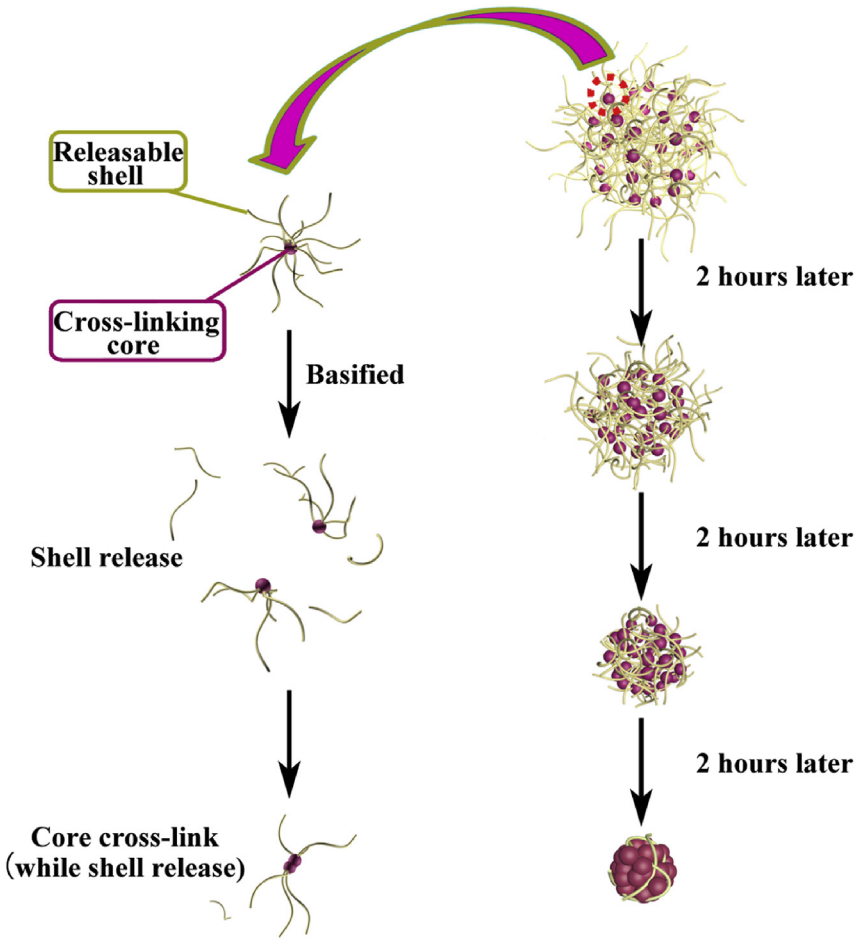

Fig. 3. The fabrication process of loose and compact nanogels.

NPs, we added 50 mg of poly(acrylic acid) (PAA) (dissolved in 50 μL of deionized water) and stirred for 30 min, followed by dialysis in water to obtain pure nanogel/SiO_2/PAA NPs. The three-layered nanoparticles were characterized by TEM, DLS and X-ray photoelectron spectroscopy (XPS) (Thermo Scientific ESCALab 250Xi using 200 W monochromated Al Kα radiation. A 500 μm X-ray spot was used for XPS analysis. The base pressure in the analysis chamber was about 3 × 10-10 mbar. Typically the hydrocarbon C1s line at 284.8 eV from adventitious carbon was used for energy referencing).

2.7. Preparation of nanogel/SiO_2/PAA/HA NPs

To prepare hydroxyapatite coating on our multi-layered nanoparticles, we first prepared hydroxyapatite (HA) nanoparticles as control by dissolving 7.2 mg potassium phosphate tribasic monohydrate in 9 mL deionized water, followed by the addition of 0.5 mL of deionized water containing 8.9 mg calcium acetate hydrate. After 1 min, the mixture was centrifuged and washed by deionized water 3 times to obtain pure hydroxyapatite nanoparticles. The hydroxyapatite nanoparticles were characterized by TEM and XRD.

Following dialysis to obtain pure nanogel/SiO_2/PAA NPs as described above, 0.5 mL of deionized water containing 7.2 mg potassium phosphate tribasic monohydrate was added and stirred for 10 min. Next, 0.5 mL of deionized water containing 8.9 mg calcium acetate hydrate was injected. After 1 min, the mixture was centrifuged and washed with deionized water three times to obtain pure nanogel/SiO_2/PAA/HA NPs, which were then characterized TEM, DLS and XRD.

2.8. Degradation and release studies of the loose and compact nanogels

A series of nanogels were prepared as described above. The *in-vitro* degradation tests of the loose and compact nanogels after cross-linking times of 4, 6, 8 and 10 h were evaluated in 1 × Phosphate Buffered Saline (PBS) containing 5 mM GSHto mimic intracellular compartments of cells. In detail, after a stable mini-emulsion of the organic mixture was obtained, 5 mL of 1 × PBS containing 5 mM GSH was added to terminate the gelation and to investigate the degradation of the nanogels. Isolation of the nanogels was performed as above, dialyzed by 1 × PBS containing 5 mM GSH for predetermined time, and then further dialyzed by deionized water for 3 days to obtain the degraded products of the nanogels. Various degradation times were applied, and studied with TEM.

To study bovine serum albumin (BSA) release from nanogel/Silicon dioxide (SiO_2) NPs, pure and surfactant-free nanogels obtained above were dialyzed by deionized water for 30 min, and then mixed with 2 mL of 27% ammonium hydroxide. The mixture was immediately injected into 4 mL of ethanol containing 10 μL Tetraethyl orthosilicate (TEOS) and stirred at 300 rpm for 1 h to obtain BSA loaded nanogel/SiO_2 NPs. The obtained solution was dialyzed by 1 × PBS. After a predetermined time ranging from 1 to

12 h, the liquid was centrifuged at 6000 rpm for 5 min, and the BSA concentration in the buffer solution was determined by the Bradford assay, with the nanoparticles re-dispersed in 1 × PBS following each test.

To study BSA release triggered by high-frequency magnetic field (HFMF), the protocol above for BSA release studies was repeated, but a high-frequency magnetic field (HFMF) with 220 kHz was applied at a predetermined time. After the solution was centrifuged at 6000 rpm for 5 min, the BSA concentration in the buffer solution was tested using the Bradford assay, with the nanoparticles re-dispersed in 1 × PBS following each test.

2.9. Preparation of nanogel/SiO_2/PAA/HA NPs loaded with rhBMP-2 (Bone morphogenetic protein 2)

Briefly, 0.2 g of nanogel/SiO_2/PAA/HA NPs prepared with 4 and 10 h gelation cores were stirred with 1 mL of deionized water containing 3 μg of rhBMP-2 overnight, respectively. The mixture was centrifuged and washed by deionized water twice. The obtained solids were freeze-dried to obtain pure nanogel/SiO_2/PAA/HA NPs loaded with rhBMP-2. As control, 0.2 g of hydroxyapatite was stirred with 1 mL of deionized water containing 3 μg rhBMP-2 overnight. The mixture was centrifuged and washed by deionized water twice, and the obtained solids were freeze-dried to obtain pure hydroxyapatite loaded with rhBMP-2.

2.10. Preparation of the composite films

The PLGA films were doped with the four groups of nanoparticles: nanogel/SiO_2/PAA/HA NP from the 4h gelation core and loaded with rhBMP-2, its equivalent from the 10h gelation core, hydroxyapatite loaded with rhBMP-2, and pure hydroxyapatite. In detail, 0.2 g of each nanoparticles were dispersed in 1.2 g dioxane containing 0.2 g PLGA. After stirring overnight, the mixture was cast onto a polytetrafluoroethylene plate. After most of the solvent had been freeze-dried for 24 h, the obtained films were removed from polytetrafluoroethylene plates and further vacuum-dried thoroughly for 24 h. The thickness of all films was about 0.5 mm. All films were cut into 1 cm length × 0.3 cm width. The films were imaged by digital camera and field emission scanning electron microscopy (SEM, JEOL JSM-6700F microscope).

2.11. Determination of alkaline phosphatase (ALP) activity

MC3T3-E1, a mouse calvaria-derived osteoblast cell line, was purchased from Cell Culture Center, Peking Union Medical College. Cells were seeded on the four groups of PLGA films above in 24-well plates and incubated in Dulbecco's modified Eagle's medium (DMEM, Hyclone). At 3, 6, and 9 days, we aspirated the cultured medium from each sample and added 200 μL of 1% Nonidet P-40 (NP-40) solution at room temperature, incubating for 1 h. We then centrifuged the cell lysate, removing 50 μL of supernatant from each well into a 96-well plate, followed by the addition of 50 μL of 2 mg/mL p-nitrophenylphosphate (Sangon) substrate solution composed of 0.1 mol/L glycine and 1 mmol/L MgCl. Following a 30 min incubation time at 37 °C, the reaction was quenched with 100 μL of 0.1 N NaOH. ALP activity was quantified by reading the absorbance at 405 nm on a microplate reader (SPECTRA max 384, Molecular Devices). The total protein content in cell lysates was determined using the bicinchoninic acid method in aliquots of the above samples with the Pierce protein assay kit (Pierce Biotechnology Inc., Rockford, IL), measured at 562 nm and calculated according to a series of albumin (bovine serum albumin) standards. The ALP levels were normalized to the total protein content. All experiments were performed in quadruple.

2.12. Ectopic bone formation

The mouse gastrocnemius pocket model was employed to examine the ectopic bone formation of the four groups of films above. Eighteen male mice (eight weeks old, Silaike Inc. Shanghai, China) were divided into 2 groups and anaesthetized with xylazine (0.02 g/kg, Sigma) and ketamine (0.1 g/kg, Sigma). Mice of group A were implanted with film fabricated with rhBMP-2 loaded nanogel/SiO_2/PAA/HA NP from the 4 h gelation core in the gastrocnemius pouch of its rear left leg, and the 10 h equivalent was implanted respectively in its right leg. Mice of group B were implanted with the rhBMP-2 loaded PLGA/HA film in the gastrocnemius pouch of its left leg, and the negative control PLGA/HA film in the respective left leg. The incision sites were then closed around the implants with resorbable continuous sutures. At 2, 4 and 6 weeks after implantation, the mice were anaesthetized by intraperitoneal injection of pentobarbital (0.06 g/kg) and scanned using X-ray (LX-60 DC12, Faxitron, 48 kv, 0.28 mA, 9.75 ms) to evaluate ectopic bone formation. The mice were then sacrificed with an overdose of pentobarbital ($n = 6$ for each material and time period) to retrieve the implants. Micro−computed tomography (micro-CT) measurements and digital photos were performed on the harvested implants and ectopic bone with a sample-to-detector distance of 1.6 m.

Histological evaluation was then performed by fixation with 4% neutral buffered formalin for 48 h, followed by decalcification of the ectopic bone samples in 12.5% ethylenediaminetetraacetic acid, dehydrated in a graded series of alcohol, and embedded in paraffin. Serial sections were then stained with hematoxylin-eosin (HE), and images were captured under light microscopy.

3. Results

3.1. Evaluation of loose and compact nanogels as a template for multilayered composites

Adjustment of gelation times from 4 to 10 h produced stable nanogels with sizes from 140 to 80 nm, confirmed by transmission electron microscopy (TEM) images (Fig. 4a) and dynamic light scattering (DLS) (Fig. 5). The biodegradable properties of these nanogel templates were correlated as a function of crosslinking times. All these hydrogels demonstrated excellent biodegradability through the cleavage of disulfide bonds by glutathione (GSH), and compacter nanogels with longer gelation time resulted in slower degradation rates (Fig. S1).

The structures and sizes of the resulting nanogel/SiO_2 NPs were heavily dependent on the type of nanogel template used (loose versus compact) (Fig. 4a, 2). Furthermore, etching the template core imparted varying degrees of porosity onto the resulting SiO_2 capsules [18,19], where loose nanogel templates translated to highly porous, sponge-like SiO_2 shells while compact nanogel templates translated to thin and compact shell walls (Fig. 4a). It is likely that TEOS readily penetrate through the matrix of loose nanogel templates during sol-gel reactions, resulting in thick, porous SiO_2 shells, with significant implications in drug delivery. Indeed, release studies of the nanogel/SiO_2 NPs using bovine serum albumin (BSA) revealed that drug loading and release properties correlated with the type of nanogel template employed during fabrication, such that the loose nanogel templates produced nanogel/SiO_2 NPs with higher drug loading capacity while the compact nanogel templates led to slower rates of drug release (i.e. better drug retention) (Fig. 6a), demonstrating excellent control over functional properties at the nanoscale level.

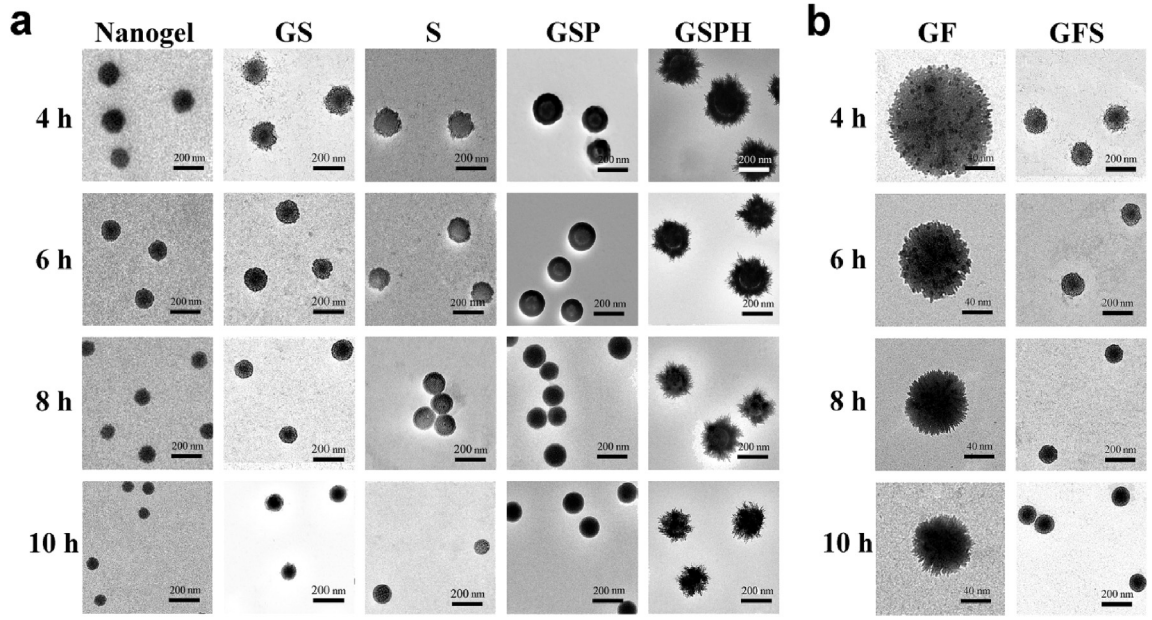

Fig. 4. Characterization of various multilayered composite nanoparticles, demonstrating fine control over structure and morphology of each layer. a) TEM images of the nanogel core (Nanogel), nanogel-silica NPs (GS), silica capsules (S), PAA-silica-nanogel NPs (GSP), and HA-PAA-silica-nanogel NP (GSPH). b) TEM images of magnetic nanogel NPs (GF) and magnetic silica-nanogel NPs (GFS).

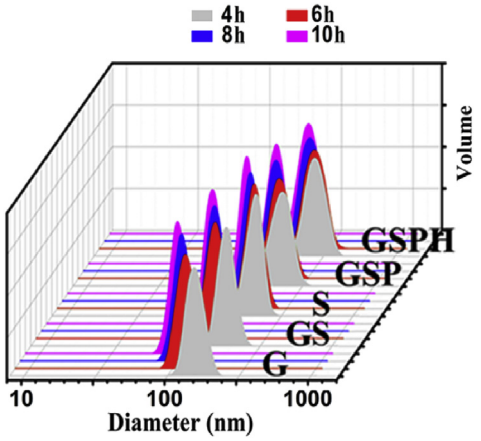

Fig. 5. Dynamic light scattering (DLS) results of multilayered composite nanoparticles. Legend: 4 h = NPs obtained from 4 h gelation time of the template.

3.2. Magnetic-sensitive nanoparticles

TEM images showed that Fe_3O_4 particles (dark dots) (Fig. S2) embedded evenly throughout the nanogel template, despite little change in particle size (Fig. 4b). Even with silica coating, the resulting magnetic silica-nanogel NPs likewise displayed little change in size or morphology compared to its nonmagnetic counterpart (Fig. 4b). Magnetic field curves for magnetic nanogel/SiO_2 NPs, showing that magnetic field curves and parametric properties were not affected by the type of template core used (Fig. S3). The magnetic nanogel/SiO_2 NPs responded well to high-frequency alternating magnetic fields (HFMF) to burst release loaded BSA (Fig. 1b) [20], while its BSA release profile in the absence of magnetic stimuli was similar to that of its nonmagnetic counterpart (Fig. 6a). However, magnetic nanogel/SiO_2 NPs formed from compact nanogel templates exhibited lower magnetic strength, likely due to less overall NP content as supported by TGA (Fig. S4). Thus shorter gelation times during fabrication led to higher magnetic field strength and greater response to HFMF stimuli, resulting in faster burst release of loaded BSA (Fig. 6b). The reliability of these magnetic field-responsive behaviors was further confirmed by applying HFMF for 10 min at three specific intervals. The release profiles, regardless of the template core used, showed burst release precisely corresponding to each application of HFMF, immediately returning to slow release following each magnetic excitation (Fig. 6c).

3.3. Multilayered composite nanoparticles with pH-sensitive release and HA coating

With deeper understanding of the design criteria required to fabricate stimuli-responsive and bio-functional multilayered composite NPs, we next sought to design a smart drug carrier with superior drug loading capacity and therapeutic performance. Specifically, we aimed to integrate additional layers with pH-responsive functionality for targeted drug release.

The resulting tri-layered nanogel/SiO_2/PAA NPs were characterized by TEM imaging (Fig. 4a), DLS (Fig. 5), and XPS spectra (Fig. S5), showing the presence of PAA as a thick layer (~10 nm) surrounding the silica coated NPs regardless of the nanogel template used. We then demonstrated pH-responsive drug delivery with these nanoparticles by measuring BSA release in various buffered solutions. Interestingly, the BSA release profile of the nanogel/SiO_2/PAA NP was much slower than its nanogel/SiO_2 equivalent in HCl-KCl buffer (at pH 1.2) (Fig. 6a,d). In fact, BSA release from the nanogel/SiO_2/PAA NP was minimal in the first five hours, and only reached 8–16% within 12 h (Fig. 6d). The same study in phosphate buffer (pH 7.4) showed similar release profiles for both NPs (Fig. 6e). Furthermore, shorter gelation times of the nanogel template led to the fabrication of nanogel/SiO_2/PAA NPs with greater responsiveness to pH stimuli (Fig. 6d). To explain these trends, we propose that under acidic conditions the outer PAA coating tightly entrap drugs loaded in the porous silica layer, enabling high drug retention (Fig. 1c). Under mild to neutral

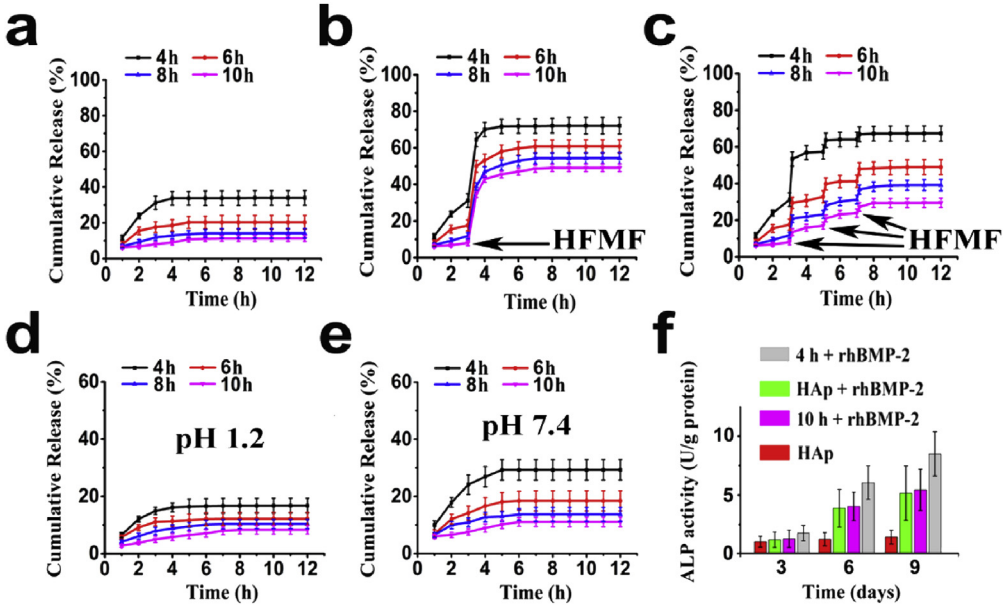

Fig. 6. Cumulative BSA release profiles of various (a) nanogel/SiO_2 NPs, Fe_3O_4-loaded nanogel/SiO_2 NPs triggered by (b) a 30 min high-frequency alternating magnetic fields (HFMF) at the 180 min mark, and (c) a 10 min HFMF stimulation applied at the three specific times (at 3, 5 and 7 h), and nanogel/SiO_2/PAA NPs at (d) pH 1.2 and (e) pH 7.4. (f) ALP activity after 3, 6 and 9 days of culture with various composite biofilms. Legend: 4h or 10h + rhBMP-2 = film fabricated using nanogel/SiO_2/PAA/HA NPs based on the 4h or 10h nanogel template loaded with rhBMP-2; HAp + rhBMP-2 = positive control of PLGA/HA film loaded with rhBMP-2; HAp = negative control of PLGA/HA film without rhBMP-2.

conditions (above pH 5.35), the carboxyl groups of PAA are partially or fully deprotonated and therefore repel [21,22], resulting in swelling of the linear PAA chains and dissociation of the PAA shell, releasing drugs from within. Importantly, our design strategy for "smart" drug delivery vehicles enables fine-tuning of the responsiveness to pH-stimuli. As we shorten the gelation time to create a more porous silica layer, polymer chains of the nanogel core extend and protrude further, leading to a thicker PAA coating and thereby improving the pH-responsiveness (Fig. 4a).

We next evaluated our four-layered nanogel/SiO_2/PAA/HA NPs. A needlelike coating of calcium phosphate was observable on the nanoparticles according to TEM (Fig. 4a), and the crystalline phase of the outer calcium phosphate was confirmed by XRD spectra to be significantly close to the standard spectrum of conventional hydroxyapatite regardless of the gelation template used (from 4, 6, 8, and 10 h gelation times) (Figs. S6, S7). Particle size analysis with DLS revealed that gelation time of the nanogel cores strongly influenced the final particle size of the four-layered nanoparticles (Fig. 5), with shorter gelation times leading to larger particles.

3.4. Application of multilayered composite NPs as periosteum-mimetic films

Next, we explored alternative applications of the MC-NPs, recognizing their potential as controlled-release carriers incorporated into periosteum-mimetic films and sheets. The periosteum, a thin membrane that surrounds bone scaffolds, has recently gained spotlight for its key role in orchestrating bone remodeling processes, resulting in numerous endeavors to engineer periosteum-mimetic structures [23]. One effective strategy is to encapsulate rhBMP-2, an osteogenic soluble growth factor, into appropriate carriers for continuous, long-term release throughout the bone remodeling process. Various biocompatible carriers have been reported for this purpose, such as collagen, β-tricalcium phosphate (β-TCP), biphasic calcium phosphate (BCP), HA, and polymer composites [24]. However, collagen carriers require excessive drug dosages due to low loading efficiency [25], while ceramics such as β-TCP and HA do not meet the mechanical requirements to contour bone surfaces [24]. Several ceramic/polymer composites have been recently designed to overcome poor loading capacity and mechanical properties, yet release kinetics are still inadequate due to a large initial burst release and poorly controlled slow release thereafter [26–29].

Therefore, the HA-doped NPs were incorporated into poly(D,L-lactic-*co*-glycolic acid) (PLGA) films to improve the loading capacity and controlled release of rhBMP-2 (Fig. 1d). We evaluated the biofilms *in-vitro* and *in-vivo* for bone tissue repair compared to traditional PLGA/HA composite films loaded with rhBMP-2 as a positive control. Structural and morphological characteristics of the composite films were similar to that of PLGA/HA films (Figs. S8, S9). To evaluate osteogenic performance *in-vitro*, we monitored the alkaline phosphatase (ALP) activity of MC3T3-E1, a mouse calvaria-derived osteoblastic cell line, in Dulbecco's modified Eagle's medium (DMEM) for 3, 6, and 9 days. Thus in the absence of osteogenic factors, the negative control group of PLGA/HA lacking rhBMP-2 showed minimal ALP activity (Fig. 6f). Interestingly, the composite biofilms fabricated from 4 h gelation templates performed significantly better in osteogenic performance than the 10 h gelation equivalent and the rhBMP-2 loaded PLGA/HA control (Fig. 6f), likely due to better drug loading capacity and controlled drug release.

3.5. Evaluation of osteogenic performance of the composites biofilms in-vivo

Following, we evaluated the osteogenic performance of the composites biofilms *in-vivo* through ectopic bone formation in the mouse gastrocnemius pocket model (Fig. 7). The 4 h and 10 h gelation templates, loaded with rhBMP-2, were used to fabricate the composite biofilms as above, with positive and negative controls using PLGA/HA films with and without rhBMP-2 respectively. Excitingly, the rhBMP-2 loaded composite film from the 4h gelation template induced significantly higher density and volume of new bone formation at 2 and 4 weeks compared to the other groups in

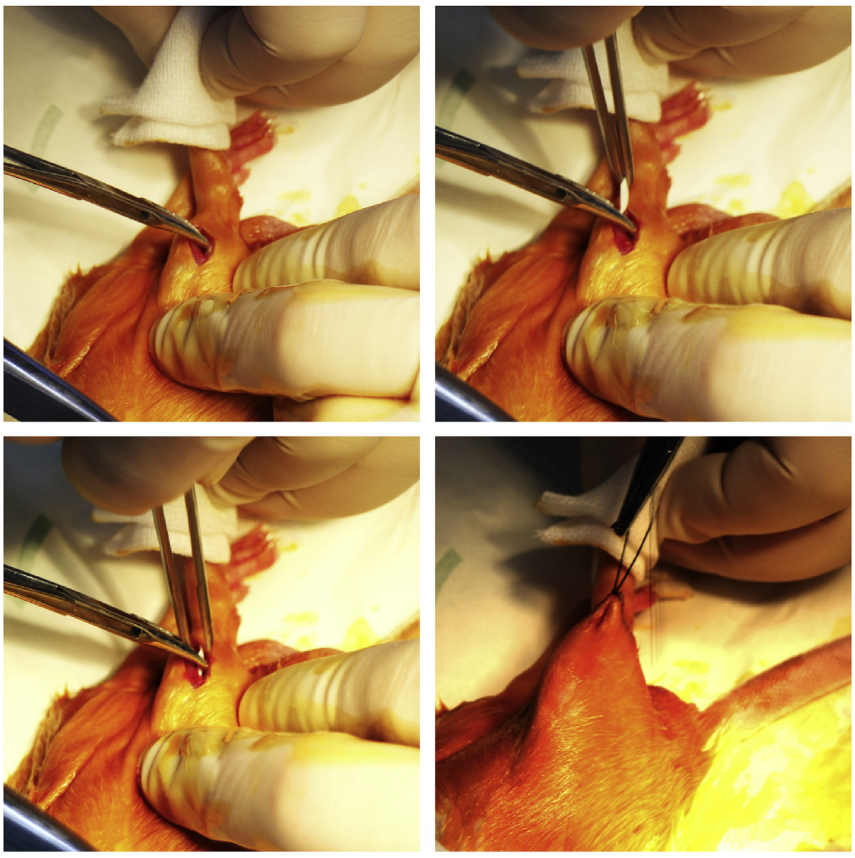

Fig. 7. Photographs of the surgical procedure.

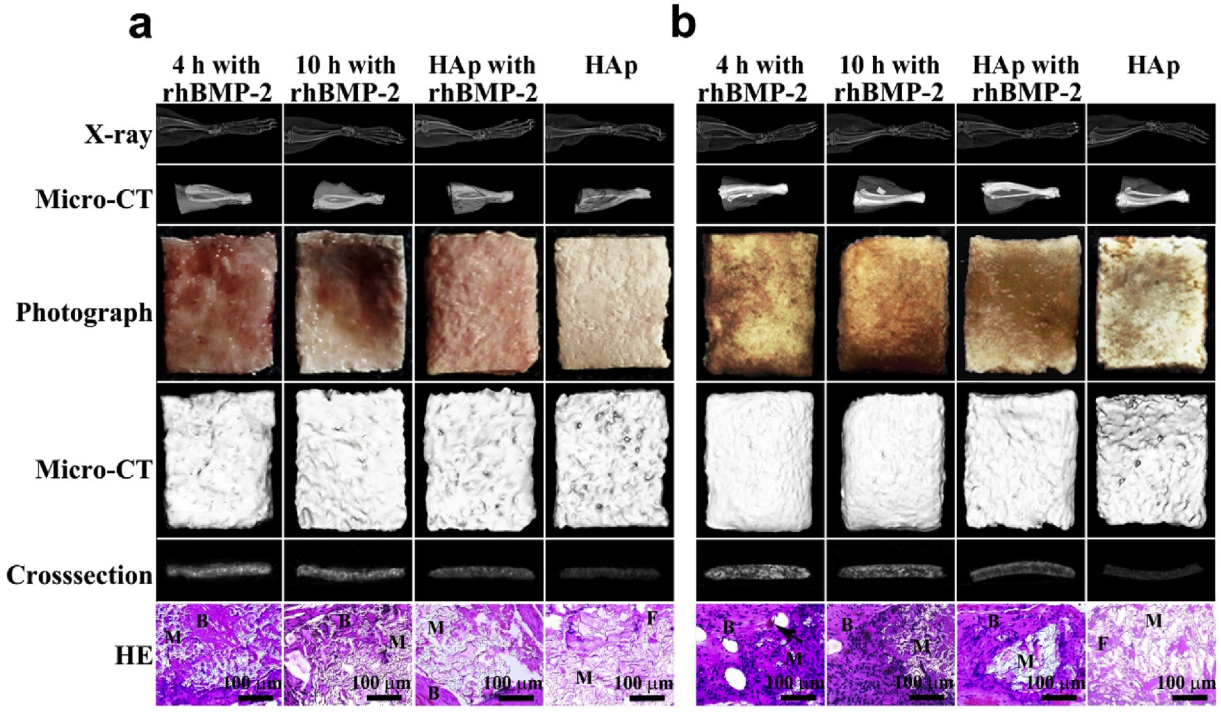

Fig. 8. X-ray, micro-CT, photograph, and H&E characterizations of ectopic bone formation in the mouse gastrocnemius pocket model after (a) 2 and (b) 4 weeks of film implantation. (B: bone, M: residual materials, F: fibrous tissue, Arrow: blood vessel).

X-ray images, digital photographs, and 3D micro-CT restructured images (Fig. 8). In fact, histological staining with H&E revealed a large amount of trabecular bone formation and minimal fibrous tissue within the ectopic bone from the 4 h gelation template group, with blood vessels even forming by 4 weeks (Fig. 8). On the other hand, the rhBMP-2 loaded composite film from the 10 h gelation template possessed slightly higher new bone formation compared to the rhBMP-2 loaded PLGA/HA film, though ectopic bone pellets produce little bone tissue. In turn, the negative control group of PLGA/HA film without rhBMP-2 showed fibrous tissue but no new bone tissue at 2 and 4 weeks. Further, the 4 h gelation template group showed superior biodegradation by 6 weeks compared to the other groups in X-ray and micro-CT (Fig. S10).

4. Discussion

To set the groundwork in a solid design platform, we induced heterogeneous growth of various functional layers onto the fine-tunable nanogel templates reported previously to produce four representative series of MC-NPs (Fig. 1a), including SiO_2 coating, pH-sensitive poly(acrylic acid) (PAA), magnetic field-sensitive Fe_3O_4, and needlelike hydroxyapatite (HA) coating.

Despite additional levels of complexity and design degrees of freedom afforded by each functional layer, controlled formation of MC-NPs was achieved by finely tunable nanogel templates, while structures and properties of each layer could be selectively designed. First, a staple of nanogel templates with varying sizes and structures were attained by inversion emulsion of a hyperbranched polymer consisting of poly(amido amine) core and poly(ethylene glycol) shell (Fig. 2), where loose nanogels were obtained by early termination of the pH-dependent thiol- disulfide exchange, and compact nanogels were obtained by late neutralization of gelation (Fig. 3). With such facile control over structural and biodegradable properties, these nanogels show promise as an ideal template for fabricating MC-NPs.

We next deposited SiO_2 coatings by the sol-gel method on selected nanogel templates to demonstrate facile control over the functional properties of subsequent layers. Assembly and hydrolysis of TEOS is widely employed to coat nanogel templates and improve the biocompatibility and stability of the nanoparticles [30–33]. Third, we implemented stimuli-responsive functionality to the nanogel/SiO_2 NPs to enable "smart", accurate, and targeted drug release by mixing Fe_3O_4 particles with the nanogel polymer prior to gelation [34–37]. These studies suggest exceptional control over drug loading capacity, drug release, and stimuli-responsive burst release to reach the therapeutic window within a short time by simply optimizing the gelation times. To achieve pH-responsive functionality, we optimized the design of the nanogel/SiO_2 core/shell NPs so that polymer chains of the nanogel would protrude through the spongy mesopore of the SiO_2 shell, exposing its positively charged amine groups onto the outer surface to allow for continuous electrostatic assembly and encapsulation of the ionizable groups by the pH-sensitive poly(acrylic acid) (PAA) [38–42]. The "smart" MC-NPs would prove particularly useful as orally administered drug delivery vehicles targeting the intestines, since the therapeutic drugs would remain well protected under the acidic conditions of the stomach. Following, we integrated a fourth layer of HA coating to improve biocompatibility of the nanogel/SiO_2/PAA NPs. We utilized the convenient anionic carboxyl groups of PAA to enable a high degree of coordination with Ca^{2+} and PO_4^{3-} to induce formation of HA crystals, resulting in a four-layered nanogel/SiO_2/PAA/HA NPs. The osteogenic results demonstrate the promising therapeutic performance of the MC-NP doped biomaterials in applications beyond drug delivery, such as for periosteum-mimetic structures for bone repair [43–46].

5. Conclusion

In summary, we have demonstrated the sequential assembly of multilayered composite NPs with a flexible nanogel template, porous silica shell of various thickness and drug release kinetics, magnetic or pH-responsive functionality, and hydroxyapatite coating. The ability to finely tune the structural and functional properties of each layer provides a rich, versatile, and powerful tool for designing "smart" and therapeutic drug carriers. This layer-by-layer technique is scalable and highly controllable, enabling streamlined work procedures for the medical treatment of oncology, digestive diseases, and orthopedics.

Acknowledgment

We gratefully acknowledge MOST (2014CB932200), "Young Thousand Talents Program", and NSFC (21674120, 81630056, 21504096, 51573195, 21474115 and 21174147) for financial support.

Appendix A. Supplementary data

Supplementary data related to this article can be found at http://dx.doi.org/10.1016/j.bioactmat.2017.06.003.

References

[1] Y. Wang, A.S. Angelatos, F. Caruso, Template synthesis of nanostructured materials via layer-by-layer assembly, Chem. Mater 20 (2007) 848–858.
[2] J. Cui, R. De Rose, K. Alt, S. Alcantara, B.M. Paterson, K. Liang, M. Hu, J.J. Richardson, Y. Yan, C.M. Jeffery, Engineering poly (ethylene glycol) particles for improved biodistribution, ACS Nano 9 (2015) 1571–1580.
[3] F. Caruso, M. Spasova, A. Susha, M. Giersig, R.A. Caruso, Magnetic nanocomposite particles and hollow spheres constructed by a sequential layering approach, Chem. Mater 13 (2001) 109–116.
[4] Y. Chen, H. Chen, D. Zeng, Y. Tian, F. Chen, J. Feng, J. Shi, Core/shell structured hollow mesoporous nanocapsules: a potential platform for simultaneous cell imaging and anticancer drug delivery, ACS Nano 4 (2010) 6001–6013.
[5] M.H. Xiong, Y. Bao, X.Z. Yang, Y.C. Wang, B. Sun, J. Wang, Lipase-sensitive polymeric triple-layered nanogel for "on-demand" drug delivery, J. Am. Chem. Soc. 134 (2012) 4355–4362.
[6] S. Mitragotri, D.G. Anderson, X. Chen, E.K. Chow, D. Ho, A.V. Kabanov, J.M. Karp, K. Kataoka, C.A. Mirkin, S.H. Petrosko, Accelerating the translation of nanomaterials in biomedicine, ACS Nano 9 (2015) 6644–6654.
[7] Z.K. Wang, D. Wang, H. Wang, J.J. Yan, Y.Z. You, Z.G. Wang, Preparation of biocompatible nanocapsules with temperature-responsive and bioreducible properties, J. Mater. Chem. 21 (2011) 15950–15956.
[8] X.J. Loh, Supramolecular host–guest polymeric materials for biomedical applications, Mater. Horiz. 1 (2014) 185–195.
[9] I. Berndt, J.S. Pedersen, W. Richtering, Structure of multiresponsive "intelligent" core-shell microgels, J. Am. Chem. Soc. 127 (2005) 9372–9373.
[10] I. Berndt, C. Popescu, F.J. Wortmann, W. Richtering, Mechanics versus thermodynamics: swelling in multiple-temperature-sensitive core–shell microgels, Angew. Chem. Int. Ed. 45 (2006) 1081–1085.
[11] R. Ghosh Chaudhuri, S. Paria, Core/shell nanoparticles: classes, properties, synthesis mechanisms, characterization, and applications, Chem. Rev. 112 (2011) 2373–2433.
[12] R.A. Caruso, A. Susha, F. Caruso, Multilayered titania, silica, and laponite nanoparticle coatings on polystyrene colloidal templates and resulting inorganic hollow spheres, Chem. Mater 13 (2001) 400–409.
[13] C. Niu, B. Zou, Y. Wang, L. Chen, H. Zheng, S. Zhou, The template-assisted synthesis of polypyrrole hollow microspheres with a double-shelled structure, Chem. Commun. 51 (2015) 5009–5012.
[14] X. Xu, S. Lü, C. Gao, X. Bai, C. Feng, N. Gao, M. Liu, Multifunctional drug carriers comprised of mesoporous silica nanoparticles and polyamidoamine dendrimers based on layer-by-layer assembly, Mater. Des. 88 (2015) 1127–1133.
[15] D.C. Wu, X.J. Loh, Y.L. Wu, C.L. Lay, Y. Liu, 'Living'controlled in situ gelling systems: thiol– disulfide exchange method toward tailor-made biodegradable hydrogels, J. Am. Chem. Soc. 132 (2010) 15140–15143.
[16] J. Zhang, F. Yang, H. Shen, D. Wu, Controlled formation of microgels/nanogels from a disulfide-linked core/shell hyperbranched polymer, ACS Macro Lett. 1 (2012) 1295–1299.
[17] P. Mongondry, C. Bonnans-Plaisance, M. Jean, J.F. Tassin, Mild synthesis of amino-poly (ethylene glycol) s. application to steric stabilization of clays, Macromol. Rapid Commun. 24 (2003) 681–685.
[18] J.F. Chen, H.M. Ding, J.X. Wang, L. Shao, Preparation and characterization of porous hollow silica nanoparticles for drug delivery application, Biomaterials 25 (2004) 723–727.

[19] Z.Z. Li, L.X. Wen, L. Shao, J.-F. Chen, Fabrication of porous hollow silica nanoparticles and their applications in drug release control, J. Control. Release 98 (2004) 245–254.
[20] S.H. Hu, T.Y. Liu, H.Y. Huang, D.M. Liu, S.Y. Chen, Magnetic-sensitive silica nanospheres for controlled drug release, Langmuir 24 (2008) 239–244.
[21] X. Yin, A.S. Hoffman, P.S. Stayton, Poly (N-isopropylacrylamide-co-propylacrylic acid) copolymers that respond sharply to temperature and pH, Biomacromolecules 7 (2006) 1381–1385.
[22] K. Lu, M. Cao, W. Mao, X. Sun, J. Tang, Y. Shen, M. Sui, Targeted acid-labile conjugates of norcantharidin for cancer chemotherapy, J. Mater. Chem. 22 (2012) 15804–15811.
[23] X. Shi, T. Fujie, A. Saito, S. Takeoka, Y. Hou, Y. Shu, M. Chen, H. Wu, A. Khademhosseini, Periosteum-mimetic structures made from freestanding microgrooved nanosheets, Adv. Mater 26 (2014) 3290–3296.
[24] S. Itoh, M. Kikuchi, K. Takakuda, Y. Koyama, H.N. Matsumoto, S. Ichinose, J. Tanaka, T. Kawauchi, K. Shinomiya, The biocompatibility and osteoconductive activity of a novel hydroxyapatite/collagen composite biomaterial, and its function as a carrier of rhBMP-2, J. Biomed. Mater. Res. 54 (2001) 445–453.
[25] H. Schliephake, H.A. Weich, C. Dullin, R. Gruber, S. Frahse, Mandibular bone repair by implantation of rhBMP-2 in a slow release carrier of polylactic acid-an experimental study in rats, Biomaterials 29 (2008) 103–110.
[26] J.H. Lee, M.Y. Ryu, H.R. Baek, J.H. Seo, K.M. Lee, J.H. Lee, Generation of an rhBMP-2-loaded beta-tricalcium phosphate/hydrogel composite and evaluation of its efficacy on peri-implant bone formation, Biomed. Mater 9 (2014) 055002.
[27] A.B. Kutikov, J.D. Skelly, D.C. Ayers, J. Song, Templated repair of long bone defects in rats with bioactive spiral-wrapped electrospun amphiphilic polymer/hydroxyapatite scaffolds, ACS Appl. Mater. Interfaces 7 (2015) 4890–4901.
[28] L. Zheng, F. Yang, H. Shen, X. Hu, C. Mochizuki, M. Sato, S. Wang, Y. Zhang, The effect of composition of calcium phosphate composite scaffolds on the formation of tooth tissue from human dental pulp stem cells, Biomaterials 32 (2011) 7053–7059.
[29] J. Zhang, J. Jia, J.P. Kim, H. Shen, F. Yang, Q. Zhang, M. Xu, W. Bi, X. Wang, J. Yang, Ionic colloidal molding as a biomimetic scaffolding strategy for uniform bone tissue regeneration, Adv. Mater (2017), http://dx.doi.org/10.1002/adma.201605546.
[30] F. Caruso, R.A. Caruso, H. Möhwald, Nanoengineering of inorganic and hybrid hollow spheres by colloidal templating, Science 282 (1998) 1111–1114.
[31] Z. Teng, X. Su, Y. Zheng, J. Zhang, Y. Liu, S. Wang, J. Wu, G. Chen, J. Wang, D. Zhao, A facile multi-interface transformation approach to monodisperse multiple-shelled periodic mesoporous organosilica hollow spheres, J. Am. Chem. Soc. 137 (2015) 7935–7944.
[32] X. Li, L. Zhou, Y. Wei, A.M. El-Toni, F. Zhang, D. Zhao, Anisotropic growth-induced synthesis of dual-compartment Janus mesoporous silica nanoparticles for bimodal triggered drugs delivery, J. Am. Chem. Soc. 136 (2014) 15086–15092.
[33] Y. Tian, A. Glogowska, W. Zhong, T. Klonisch, M. Xing, Polymeric mesoporous silica nanoparticles as a pH-responsive switch to control doxorubicin intracellular delivery, J. Mater. Chem. 1 (2013) 5264–5272.
[34] D. Ho, X. Sun, S. Sun, Monodisperse magnetic nanoparticles for theranostic applications, Acc. Chem. Res. 44 (2011) 875–882.
[35] R. Hao, R. Xing, Z. Xu, Y. Hou, S. Gao, S. Sun, Synthesis, functionalization, and biomedical applications of multifunctional magnetic nanoparticles, Adv. Mater 22 (2010) 2729–2742.
[36] J. Kim, J.E. Lee, S.H. Lee, J.H. Yu, J.H. Lee, T.G. Park, T. Hyeon, Designed fabrication of a multifunctional polymer nanomedical platform for simultaneous cancer-targeted imaging and magnetically guided drug delivery, Adv. Mater 20 (2008) 478–483.
[37] Y. Chen, J. Nan, Y. Lu, C. Wang, F. Chu, Z. Gu, Hybrid Fe_3O_4-Poly (acrylic acid) nanogels for theranostic cancer treatment, J. Biomed. Nanotechnol. 11 (2015) 771–779.
[38] S.W. Song, K. Hidajat, S. Kawi, pH-controllable drug release using hydrogel encapsulated mesoporous silica, Chem. Commun. (2007) 4396–4398.
[39] S. Simovic, C.A. Prestidge, Nanoparticle layers controlling drug release from emulsions, Eur. J. Pharm. Biopharm. 67 (2007) 39–47.
[40] X.Z. Yang, X.J. Du, Y. Liu, Y.H. Zhu, Y.Z. Liu, Y.P. Li, J. Wang, Rational design of polyion complex nanoparticles to overcome cisplatin resistance in cancer therapy, Adv. Mater 26 (2014) 931–936.
[41] W. Sun, T. Jiang, Y. Lu, M. Reiff, R. Mo, Z. Gu, Cocoon-like self-degradable DNA nanoclew for anticancer drug delivery, J. Am. Chem. Soc. 136 (2014) 14722–14725.
[42] M. Wang, K. Alberti, S. Sun, C.L. Arellano, Q. Xu, Combinatorially designed lipid-like nanoparticles for intracellular delivery of cytotoxic protein for cancer therapy, Angew. Chem. 126 (2014) 2937–2942.
[43] Y. Kang, L. Ren, Y. Yang, Engineering vascularized bone grafts by integrating a biomimetic periosteum and β-TCP scaffold, ACS Appl. Mater. Interfaces 6 (2014) 9622–9633.
[44] M.D. Hoffman, D.S. Benoit, Emulating native periosteum cell population and subsequent paracrine factor production to promote tissue engineered periosteum-mediated allograft healing, Biomaterials 52 (2015) 426–440.
[45] M.D. Hoffman, C. Xie, X. Zhang, D.S. Benoit, The effect of mesenchymal stem cells delivered via hydrogel-based tissue engineered periosteum on bone allograft healing, Biomaterials 34 (2013) 8887–8898.
[46] S.J. Roberts, N. van Gastel, G. Carmeliet, F.P. Luyten, Uncovering the periosteum for skeletal regeneration: the stem cell that lies beneath, Bone 70 (2015) 10–18.